Universal anomalous diffusion of quantized vortices in ultra-quantum turbulence

Satoshi Yui, ^{1,*} Yuan Tang, ^{2,3,*} Wei Guo, ^{2,3,†} Hiromichi Kobayashi, ^{4,5,‡} and Makoto Tsubota ^{6,§}

¹Department of Physics, Osaka Metropolitan University,
3-3-138 Sugimoto, Sumiyoshi-ku, Osaka 558-8585, Japan

²National High Magnetic Field Laboratory, 1800 East Paul Dirac Drive, Tallahassee, Florida 32310, USA

³Mechanical Engineering Department, FAMU-FSU College of Engineering,
Florida State University, Tallahassee, Florida 32310, USA

⁴Research and Education Center for Natural Sciences, Keio University,
4-1-1 Hiyoshi, Kohoku-ku, Yokohama 223-8521, Japan

⁵Department of Physics, Keio University, 4-1-1 Hiyoshi, Kohoku-ku, Yokohama 223-8521, Japan

⁶Department of Physics & Nambu Yoichiro Institute of Theoretical and Experimental Physics
(NITEP) & The OCU Advanced Research Institute for Natural Science and Technology (OCARINA),
Osaka Metropolitan University, 3-3-138 Sugimoto, Sumiyoshi-ku, Osaka 558-8585, Japan
(Dated: May 14, 2022)

In classical viscous fluids, turbulent eddies are known to be responsible for the rapid spreading of embedded particles. But in inviscid quantum fluids where the turbulence is induced by a chaotic tangle of quantized vortices, dispersion of the particles can be achieved via a non-classical mechanism, i.e., their binding to the evolving vortices. However, knowledge on how the vortices diffuse and spread in quantum-fluid turbulence is very limited, especially for the so-called ultra-quantum turbulence (UQT) generated by a random tangle of vortices. Here we report a systematic numerical study of the apparent diffusion of vortices in UQT in superfluid helium-4 using the full Biot-Savart simulation. We reveal that the vortices in the superfluid exhibit a universal anomalous diffusion (superdiffusion) at small times, which transits to normal diffusion at large times. This behavior is found to be the result of a generic scaling property of the vortex velocity. Our simulation at finite temperatures also nicely reproduces recent experimental observations. The knowledge obtained from this study may form the base for understanding turbulent transport and universal vortex dynamics in various quantum fluids.

Turbulent diffusion in classical fluids has been studied extensively due to its wide range of applications such as chemical mixing in star formation [1] and airborne virus transmission [2]. It has been known that the turbulent eddies can carry embedded particles, leading to some well-known time scaling of the particle separation such as the Richardson's t^3 law [3]. However, this knowledge does not apply to inviscid quantum fluids such as superfluid helium-4 (He II) and atomic Bose-Einstein condensates (BECs), since the injected particles are not entrained by the superfluid flow at low temperatures. Instead, a distinct transport mechanism exists, i.e., binding to the evolving quantized vortices.

In a quantum fluid, turbulence can be induced by a chaotic tangle of quantized vortex lines [4], which are line-shaped topological defects featured by a circulating flow with a quantized circulation $\kappa = h/m$, where h is Plank's constant and m is the mass of the bosons constituting the superfluid [5]. The vortices evolve with time chaotically, and they also undergo reconnections when they move across each other [6]. Depending on the internal structure of the vortex tangle, two forms of turbulent flows may emerge in a quantum fluid [7, 8]. The first form is called quasiclassical turbulence where the vortices in the tangle can polarize locally and form bundles to mimic classical vortices [9]. In this case, the induced velocity field can exhibit various classical features at length scales greater than the mean vortex-line spacing

 ℓ [10, 11]. On the other hand, when the vortices in the tangle arrange themselves randomly, an ultra-quantum turbulence (UQT) with no classical analogue is generated, where the flow field fluctuates at scales comparable to ℓ without any large-scale motion [12]. Particles in a quantum fluid can bind to the vortex cores and subsequently move together with the vortices [13–16]. Knowing how vortices diffuse in space is therefore crucial for understanding turbulent transport in quantum fluids.

So far, there have been very limited studies on the apparent diffusion of vortices in quantum-fluid turbulence. On the theoretical side, the overall expansion of a decaying random vortex tangle near a solid wall [17] and in bulk He II [18] was simulated. But these studies only provide limited insights into the diffusion behavior of vortices in a fully developed turbulence. In a recent experiment, Tang et al. decorated the vortices in UQT generated by counterflow in He II with solidified deuterium tracer particles. They observed that the vortices undergo anomalous diffusion (superdiffusion) at small times [19]. Their measured diffusion time exponent appears to be insensitive to both the temperature and the vortex-line density, suggesting possible generic nature of this vortex-diffusion behavior. However, since the experiment was conducted in a narrow temperature range (i.e., 1.7 K to 2.0 K), a reliable conclusion cannot be achieved.

In this paper, we report a systematic numerical study of the apparent diffusion of individual vortices in UQT

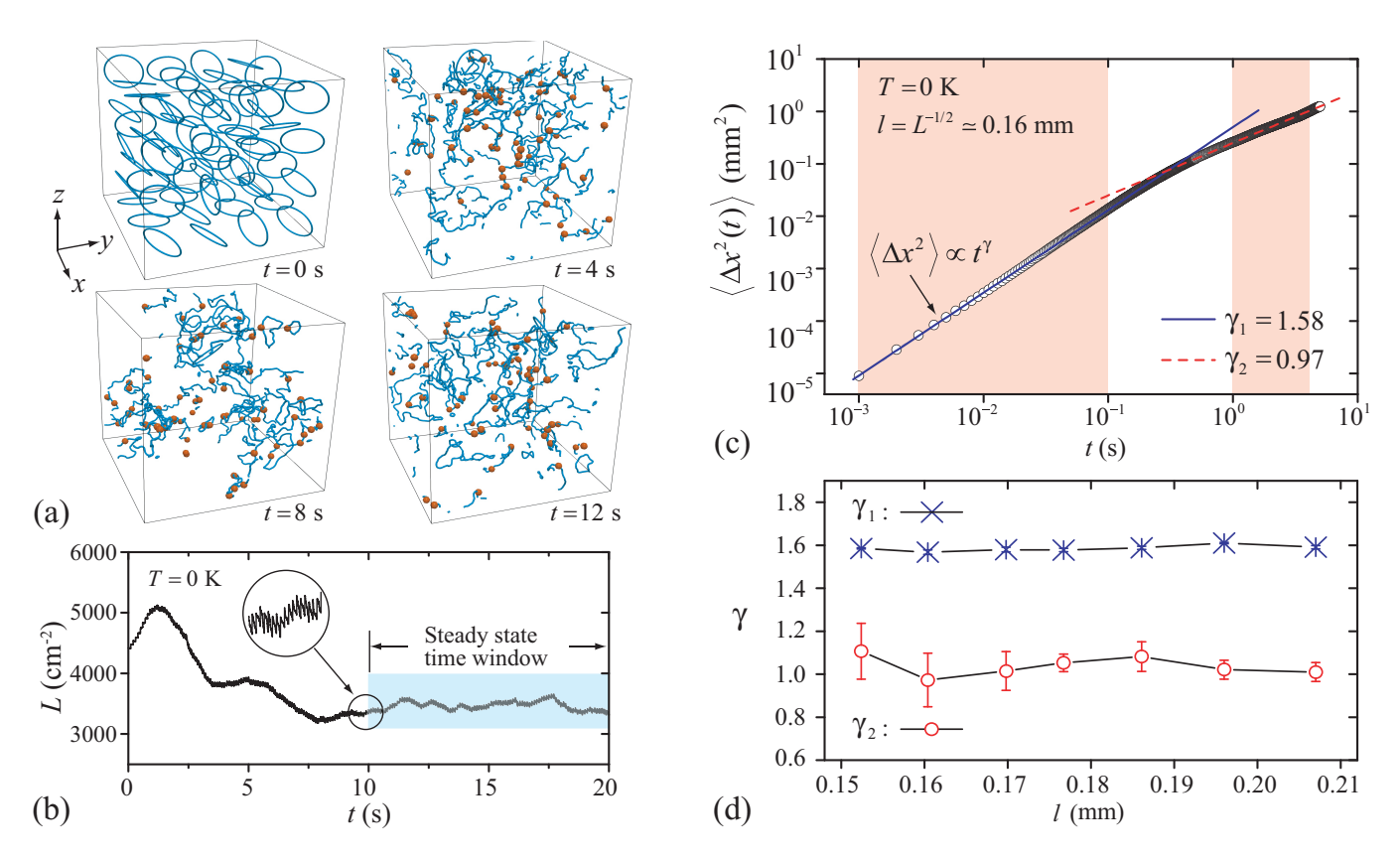


FIG. 1. (a) Snapshots of an evolving random vortex tangle. The red dots represents the vortex-filament points tracked for diffusion analysis. (b) Variation of the corresponding vortex-line density L(t). The blow-up in the inset shows fluctuations in L due to ring injections. (c) Mean square displacement of the vortices $\langle \Delta x^2(t) \rangle$ in the x direction. The solid and dashed lines are power-law fits to the data in the shaded regions. (d) Diffusion exponents γ averaged over x, y, and z directions versus the mean vortex-line spacing $\ell = L^{-1/2}$. The error bars (barely visible for γ_1) represent the standard deviations of the γ values for diffusion in the three axial directions.

in He II using the full Biot-Savart simulation [20]. We reveal that in pure superfluid the vortices in UQT indeed undergo superdiffusion at small times with a universal diffusion exponent regardless how dense the tangle At large times, the superdiffusion transits to normal diffusion due to vortex reconnections. Our analysis shows that this universal diffusion behavior is caused by a generic temporal correlation of the vortex velocity, which should exist in other quantum fluids where the Biot-Savart law applies. At finite temperatures, the viscous effect is found to only mildly affect the vortex diffusion, which nicely explains the experimental observations. Since UQT can be produced by counterflow in quantum two-fluid systems such as He II [21, 22], atomic BECs [23], and superfluid neutron stars [24, 25], and it can also spontaneously emerge following a second-order phase transition in quantum fluids via the Kibble-Zurek mechanism [26, 27], the knowledge obtained in our study may also offer valuable insights into the evolution and quenching dynamics of these diverse quantum fluids.

Vortex diffusion in a pure superfluid.—Like many other

quantum fluids, He II can be considered as a mixture of two miscible fluid components, i.e., an inviscid superfluid and a viscous normal fluid (i.e., collection of thermal quasiparticles) [28]. The normal-fluid fraction in He II drops with decreasing the temperature and becomes negligible below 1 K. Experimentally, an UQT can be produced in He II at zero-temperature limit by injecting small vortex rings [12]. Here, we adopt a similar method numerically to study vortex diffusion in UQT in pure superfluid. As shown in Fig. 1 (a), we first place 64 randomly oriented vortex rings (radius: $R_{in} = 0.11$ mm) in a cubical computational box (side length: D=1mm) with periodic boundary conditions in all three axial directions. These vortices are described by the vortex filament model [29], and each vortex filament is discretized into a series of points. In the absence of the normal fluid, a vortex-filament point at s moves at the local superfluid velocity $\mathbf{v}_s(\mathbf{s})$ as given by the Biot-Savart law [29, 30]:

$$\frac{d\mathbf{s}}{dt} = \mathbf{v}_s(\mathbf{s}) = \frac{\kappa}{4\pi} \int \frac{(\mathbf{s}_1 - \mathbf{s}) \times d\mathbf{s}_1}{|\mathbf{s}_1 - \mathbf{s}|^3}.$$
 (1)

The time evolution of the vortices can be obtained through a temporal integration of the equation (1) (see details and movies in Supplemental Materials [31], which includes additional references [32–34]). When two vortex filaments approach to have a minimum separation less than 0.008 mm, we reconnect them at the location of the minimum separation following the procedures as detailed in references [30, 35]. We also inject a randomly oriented vortex ring of radius R_{in} at a random location in the computational box with a repetition time t_{in} to balance the cascade loss of the vortices [30]. Fig. 1 (a) shows the evolution of the vortex tangle with $t_{in} = 0.08$ s. The variation of the vortex-line density L (i.e., vortex length per unit volume) is shown in Fig. 1 (b). After about 10 s, L settles to a nearly constant level. This steady-state L level can be tuned by varying t_{in} .

To study vortex diffusion, we track randomly chosen vortex-filament points and analyze their mean square displacement (MSD) along each axis (see Supplemental Materials [31]). Fig. 1 (c) shows the MSD of the vortices in the x direction $\langle \Delta x^2(t) \rangle = \langle [x(t_0 + t) - x(t_0)]^2 \rangle$ in a representative case, where t_0 is the reference time when a vortex-filament point is tracked and the angle brackets denote an ensemble average of all the tracked points in the steady state. Usually, a power-law scaling $\langle \Delta x^2(t) \rangle \propto t^{\gamma}$ is expected, where the exponent γ defines different diffusion regimes, i.e., normal diffusion $(\gamma = 1)$ and anomalous diffusion (superdiffusion at $\gamma > 1$ and subdiffusion at $\gamma < 1$) [36]. Our data exhibit a clear superdiffusion regime ($\gamma_1 = 1.58$) at small t and a normal diffusion regime ($\gamma_2 = 0.97$) at large t. Simulations conducted at other L also show similar behaviors. The derived γ_1 and γ_2 are plotted in Fig. 1 (d) as a function of the mean vortex-line spacing $\ell = L^{-1/2}$. It is clear that γ_1 is about 1.6 at all ℓ values. γ_2 is around 1 but has sizable variations in the three axial directions. These variations are caused by the reduced sample numbers at large t as well as the limited size of the computational box (see Supplemental Materials [31]).

Explanation onvortexdiffusionscaling.-Superdiffusion has been observed in various systems, such as hopping of cold atoms in an optical lattice [37] and cellular transport in biological systems [38]. For systems involving random walkers, the appearance of superdiffusion is usually attributed to Lévy flights, i.e., occasional long-distance hops of the walkers [39]. These flights lead to power-law tails of the walker's displacement distribution $P(\Delta x) \propto |\Delta x|^{-\alpha}$, which is flat enough (i.e., $\alpha < 3$) to cause superdiffusion [40]. In He II, large displacements of the vortices over short times can occur at the locations of vortex reconnections [41]. However, we find that these reconnections always result in tails of the vortex displacement distribution $P(\Delta x)$ steeper than $|\Delta x|^{-3}$ (see Supplemental Materials [31]). Therefore, they cannot account for the observed vortex superdiffusion. On the other hand, superdiffusion can

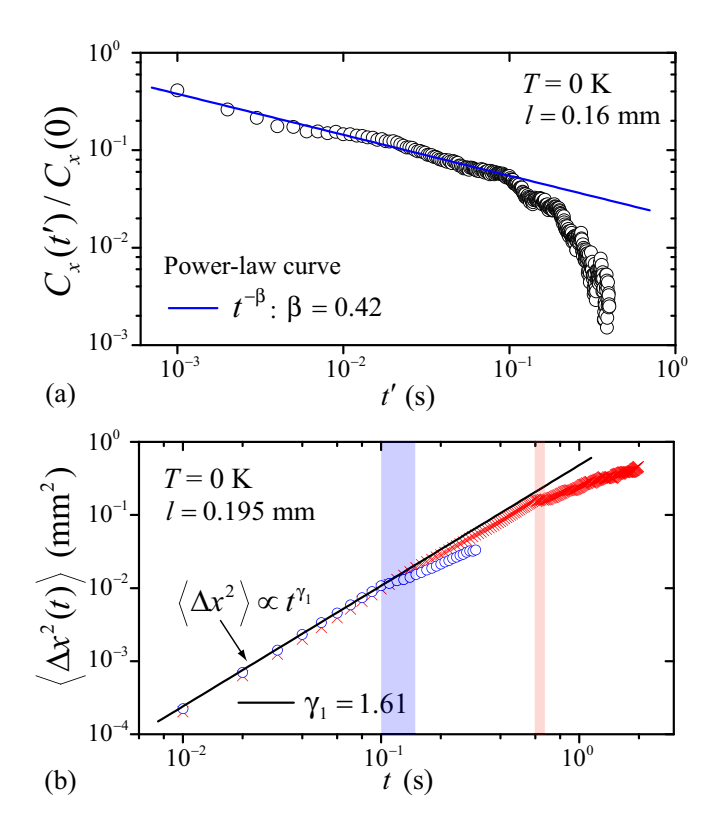


FIG. 2. (a) Vortex-velocity temporal correlation function $C_x(t')$ for a representative tangle exhibiting a power-law scaling that leads to the observed superdiffusion. (b) $\langle \Delta x^2(t) \rangle$ data for two selected groups of vortex-filament points (i.e., blue circles and red crosses) which encountered their first reconnection event in the diffusion time intervals shaded by the respective colors.

emerge if the motion of the walkers is not completely random but has extended temporal correlations [40, 42]. To see this, we write the MSD of a vortex-filament point $\langle \Delta x^2(t) \rangle$ in terms of its velocity $v_x(t)$ as [43]:

$$\langle \Delta x^2(t) \rangle = 2 \int_0^t dt_0 \int_0^{t-t_0} dt' \langle v_x(t_0) v_x(t_0 + t') \rangle. \tag{2}$$

For a fully developed random tangle, the vortex-velocity temporal correlation function $C_x(t') = \langle v_x(t_0)v_x(t_0+t') \rangle$ only depends on the lapse time t'. If $C_x(t')$ shows a power-law scaling $C_x(t') \propto t'^{-\beta}$ over a large time interval, $\langle \Delta x^2(t) \rangle$ would scale as $\langle \Delta x^2(t) \rangle \propto t^{2-\beta}$ according to equation 2 and can exhibit superdiffusion when $\beta < 1$. In Fig. 2 (a), we show the calculated $C_x(t')$ for a representative tangle with $\ell = 0.16$ mm. There is a clear power-law scaling with a fitted exponent $\beta = 0.42$, which leads to $\langle \Delta x^2(t) \rangle \propto t^{1.58}$, matching nicely the superdiffusion exponent reported in Fig. 1. Similar results are obtained for other cases at different ℓ , which confirms that the universal vortex superdiffusion at small t is caused by the temporal correlation of the vortex velocity. This correlation is an intrinsic feature of UQT.

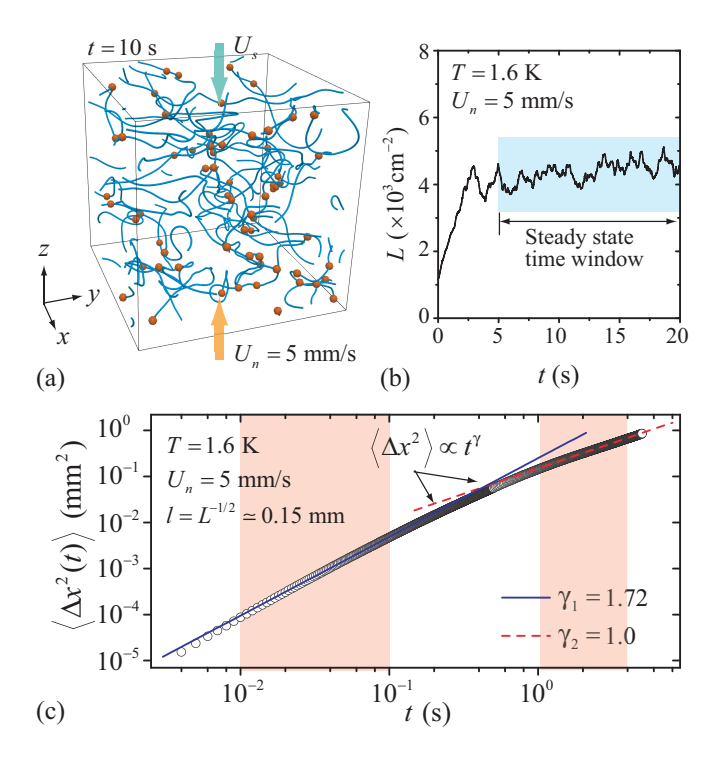


FIG. 3. (a) A representative snapshot of the vortex tangle produced by counterflow at $T=1.6~\mathrm{K}$ with $U_n=5~\mathrm{mm/s}$. The red dots represent the tracked vortex-filament points. (b) Evolution of the vortex-line density L(t). (c) Mean square displacement of the vortices in the x direction in counterflow. The solid and dashed lines are power-law fits to the data in the shaded regions.

The transition to the normal diffusion at large t was also observed experimentally by Tang $et\ al.$ [19]. They proposed that this transition is caused by vortex reconnections, which effectively randomize the motion of the participating vortex-filament points and hence suppress their velocity temporal correlation. To verify this view, we show the MSD of two selected groups of vortex-filament points for the case with $\ell=0.195$ mm in Fig. 2 (b). These two groups encountered their first reconnection event in the diffusion time interval t=0.1-0.15 s and t=0.6-0.65 s, respectively. Obvious deviation from the superdiffusion scaling is observed for each group following the reconnection event, which clearly proves the causality between vortex reconnections and the transition towards the normal diffusion.

Finite-temperature effect.—At finite temperatures, the vortices experience a drag force as they move through the normal fluid due to scattering of the thermal quasiparticles in He II [44]. The velocity of a vortex-filament point at **s** is now given by [29, 30]:

$$d\mathbf{s}/dt = \mathbf{v}_s(\mathbf{s}) + \alpha \mathbf{s}' \times (\mathbf{v}_n - \mathbf{v}_s) - \alpha' \mathbf{s}' \times [\mathbf{s}' \times (\mathbf{v}_n - \mathbf{v}_s)], (3)$$

where α and α' are temperature dependant mutual friction coefficients [45], \mathbf{s}' is the unit tangent vector along

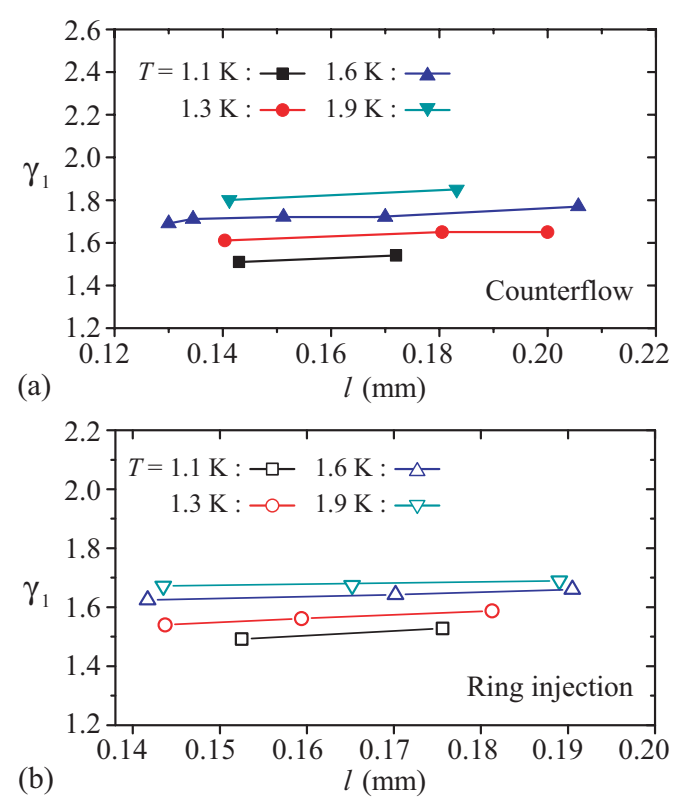


FIG. 4. (a) Diffusion exponent γ_1 versus ℓ for vortex tangles produced by counterflow at various T. (b) γ_1 versus ℓ for tangles produced by vortex-ring injection.

the filament, and \mathbf{v}_n is the normal-fluid velocity. We then generate a steady-state vortex tangle using two distinct methods. The first method is the same as the one adopted at 0 K, i.e., by randomly injecting small vortex rings in the computational box with static normal fluid (i.e., $\mathbf{v}_n = 0$). The second method is via thermal counterflow as adopted in Tang et al's experiment [19].

In He II, a counterflow can be generated by an applied heat flux q, where the normal fluid moves in the heat flow direction at a mean velocity $U_n = q/\rho sT$ while the superfluid moves oppositely at $U_s = (\rho_n/\rho_s)U_n$ [28]. Here, $\rho = \rho_n + \rho_s$ is the total density, and s is the He II specific entropy [46]. To compare with the experiment where the normal-fluid flow is laminar, we set $\mathbf{v}_n = U_n \hat{\mathbf{e}}_z$ and \mathbf{v}_s as the sum of $-U_s \hat{\mathbf{e}}_z$ and the induced velocity given in equation (1). We then place a few randomly oriented seed vortex rings in the computational box. These rings can grow and reconnect, eventually leading to a fully developed tangle [20]. A snapshot of such a tangle at T = 1.6 K and $U_n = 5$ mm/s is shown in Fig. 3 (a), and the line-density evolution is given in Fig. 3 (b). In the steady-state time window (i.e., 5-20 s), we track randomly selected vortex-filament points and analyze their MSD in the directions perpendicular to the counterflow. Representative data for $\langle \Delta x^2(t) \rangle$ are shown in Fig. 3 (c). Again, a superdiffusion regime is observed at small t,

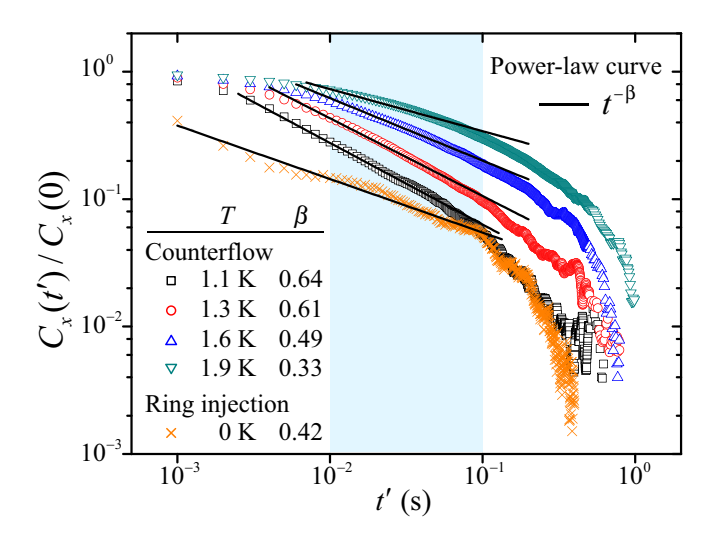


FIG. 5. Vortex-velocity temporal correlation function $C_x(t')$ at various T. The data are for tangles with ℓ of about 0.14-0.16 mm. The solid lines represent power-law fits to the data in the shaded region.

which transits to normal diffusion at large t.

In Fig. 4 (a) and (b), we collect the derived superdiffusion exponent γ_1 for tangles generated respectively by counterflow and ring injections at various ℓ and T. It is clear that γ_1 is around 1.6 nearly independent of ℓ , which is in good agreement with the experimental observations [19]. We also see that γ_1 increases by less than 0.3 from 1.1 K to 1.9 K, which is hardly resolvable in the narrow temperature range examined in the experiment. At a given T, the γ_1 value for tangles produced by counterflow is slightly larger than that for random tangles produced by ring injections. This difference becomes more visible as T increases. Interestingly, it has been known that the vortex tangle produced by counterflow becomes increasingly anisotropic as T increases [20]. This tangle anisotropy could be the origin of the observed difference, which is a topic for future research.

Discussion.—The weak temperature dependence of γ_1 indeed reflects interesting physics. To explain it, we show in Fig. 5 the normalized $C_x(t')/C_x(0)$ curves for vortex tangles produced by counterflow at various T with ℓ in the range of 0.14 - 0.16 mm. The curve for a random tangle produced by ring injections at 0 K with $\ell = 0.16$ mm is also included as a reference. Compared to the T=0 curve, a major difference of the curves at finite Tis that they saturate to 1 at larger t'. This saturation, which corresponds to ballistic motion of the vortices (i.e., $\langle \Delta x^2(t) \rangle \propto t^2$ according to equation (2)), is controlled by how the turbulent energy decays. At 0 K, the turbulent energy can cascade to scales smaller than ℓ by exciting Kelvin waves on the vortices [47]. These waves result in small-scale deformations of the vortices, which can cause rapid directional change of the vortex velocity [30] and hence suppress the velocity temporal correlation. As

such, $C_x(t')$ at 0 K remains far from saturation down to $t'=10^{-3}$ s. At finite T, the mutual friction from the normal fluid damps out the Kelvin waves and terminates the energy cascade at scales comparable to ℓ [48, 49], which results in smoother vortices. Therefore, the vortices can maintain their ballistic motion to larger t'. The extension of the ballistic region first makes the $C_x(t')/C_x(0)$ curve steeper in the power-law region, leading to a larger exponent β as compared to the 0-K case. As T further increases, the power-law region gradually shrinks and levels off, which reduces β . The decrease in β then causes γ_1 to gradually rise as observed in Fig. 4.

Y.T. and W.G. are supported by the National Science Foundation under Grant DMR-2100790 and the US Department of Energy under Grant DE-SC0020113. They also acknowledge the support and resources provided by the National High Magnetic Field Laboratory at Florida State University, which is supported by the National Science Foundation Cooperative Agreement No. DMR-1644779 and the state of Florida. S.Y. is supported by the Grant-in-Aid for JSPS Fellow program under Grant No. JP19J00967. M.T. acknowledges the support by the JSPS KAKENHI program under Grant No. JP20H01855.

- * Equal contributions
- † Email: wguo@magnet.fsu.edu
- [‡] Email: hkobayas@keio.jp
- § Email: tsubota@osaka-cu.ac.jp
- [1] Y. Feng and M. Krumholz, "Early turbulent mixing as the origin of chemical homogeneity in open star clusters," Nature **513**, 523–525 (2014).
- [2] C. C. Wang, K. A. Prather, J. Sznitman, J. L. Jimenez, S. S. Lakdawala, Z. Tufekci, and L. C. Marr, "Airborne transmission of respiratory viruses," Science 373, eabd9149 (2021).
- [3] K. R. Sreenivasan, "Turbulent mixing: A perspective," Proc. Natl. Acad. Sci. U.S.A 116, 18175–18183 (2019).
- [4] W. F. Vinen and J. J. Niemela, "Quantum turbulence," J. Low Temp. Phys. 128, 167–231 (2002).
- [5] D. R. Tilley and J. Tilley, Superfluidity and Superconductivity, 3rd ed. (Institute of Physics, Bristol, 1990).
- [6] J. Koplik and H. Levine, "Vortex reconnection in super-fluid helium," Phys. Rev. Lett. 71, 1375–1378 (1993).
- [7] G. E. Volovik, "Classical and quantum regimes of superfluid turbulence," JETP Lett. **78**, 533–537 (2003).
- [8] P. Walmsley, D. Zmeev, F. Pakpour, and A. Golov, "Dynamics of quantum turbulence of different spectra," Proc. Natl. Acad. Sci. U.S.A 111, 4691–4698 (2014).
- [9] A. W. Baggaley, J. Laurie, and C. F. Barenghi, "Vortexdensity fluctuations, energy spectra, and vortical regions in superfluid turbulence," Phys. Rev. Lett. 109, 205304 (2012).
- [10] Y. Tang, S. Bao, T. Kanai, and W. Guo, "Statistical properties of homogeneous and isotropic turbulence in He II measured via particle tracking velocimetry," Phys. Rev. Fluids 5, 084602 (2020).

- [11] Y. Tang, W. Guo, V. S. L'vov, and A. Pomyalov, "Eulerian and lagrangian second-order statistics of superfluid ⁴He grid turbulence," Phys. Rev. B 103, 144506 (2021).
- [12] P. M. Walmsley and A. I. Golov, "Quantum and quasiclassical types of superfluid turbulence," Phys. Rev. Lett. 100, 245301 (2008).
- [13] L. F. Gomez et al., "Shapes and vorticities of superfluid helium nanodroplets," Science 345, 906–909 (2014).
- [14] G. P. Bewley, D. P. Lathrop, and K. R. Sreenivasan, "Superfluid helium: Visualization of quantized vortices," Nature 441, 588 (2006).
- [15] D. E. Zmeev, F. Pakpour, P. M. Walmsley, A. I. Golov, W. Guo, D. N. McKinsey, G. G. Ihas, P. V. E. McClintock, S. N. Fisher, and W. F. Vinen, "Excimers he₂ as tracers of quantum turbulence in ⁴He in the t=0 limit," Phys. Rev. Lett. **110**, 175303 (2013).
- [16] B. Mastracci and W. Guo, "Characterizing vortex tangle properties in steady-state He II counterflow using particle tracking velocimetry," Phys. Rev. Fluids 4, 023301 (2019).
- [17] M. Tsubota, T. Araki, and W. F. Vinen, "Diffusion of an inhomogeneous vortex tangle," Phys. B: Condens. Matter 329-333, 224-225 (2003).
- [18] E. Rickinson, N. G. Parker, A. W. Baggaley, and C. F. Barenghi, "Inviscid diffusion of vorticity in lowtemperature superfluid helium," Phys. Rev. B 99, 224501 (2019).
- [19] Y. Tang, S. Bao, and W. Guo, "Superdiffusion of quantized vortices uncovering scaling laws in quantum turbulence," Proc. Natl. Acad. Sci. U.S.A 118, e2021957118 (2021).
- [20] H. Adachi, S. Fujiyama, and M. Tsubota, "Steady-state counterflow quantum turbulence: Simulation of vortex filaments using the full biot-savart law," Phys. Rev. B 81, 104511 (2010).
- [21] W. F. Vinen, "Mutual friction in a heat current in liquid helium II. I. experiments on steady heat currents," Proc. Roy. Soc. A 240, 114–127 (1957).
- [22] J. Gao, W. Guo, V. S. L'vov, A. Pomyalov, L. Skrbek, E. Varga, and W. F. Vinen, "Decay of counterflow turbulence in superfluid ⁴He," JETP Lett. 103, 648–652 (2016).
- [23] H. Takeuchi, S. Ishino, and M. Tsubota, "Binary quantum turbulence arising from countersuperflow instability in two-component bose-einstein condensates," Phys. Rev. Lett. 105, 205301 (2010).
- [24] G. Greenstein, "Superfluid turbulence in neutron stars," Nature 227, 791–794 (1970).
- [25] B. Haskell, D. Antonopoulou, and C. F. Barenghi, "Turbulent, pinned superfluids in neutron stars and pulsar glitch recoveries," Mon. Notices Royal Astron. Soc. 499, 161–170 (2020).
- [26] W. H. Zurek, "Cosmological experiments in superfluidhelium?" Nature 317, 505–508 (1985).
- [27] G. W. Stagg, N. G. Parker, and C. F. Barenghi, "Ultraquantum turbulence in a quenched homogeneous bose gas," Phys. Rev. A 94, 053632 (2016).
- [28] L. D. Landau and E. M. Lifshitz, Fluid Mechanics, 2nd ed., Vol. 6 (Pergamon Press, Oxford, 1987).
- [29] K. W. Schwarz, "Three-dimensional vortex dynamics in superfluid ⁴He: Homogeneous superfluid turbulence," Phys. Rev. B 38, 2398–2417 (1988).
- [30] M. Tsubota, T. Araki, and S. K. Nemirovskii, "Dynamics of vortex tangle without mutual friction in superfluid

- ⁴He," Phys. Rev. B **62**, 11751–11762 (2000).
- [31] See Supplemental Material at http://link.aps.org/XXX for movies and further discussions of the numerical method.
- [32] W. H. Press, B. P. Flannery, S. A. Teukolsky, and W. T. Vetterling, *Numerical Recipes in C. The Art of Scientific Computing* (Cambridge University Press, Cambridge, 1992).
- [33] A. C. White, C. F. Barenghi, N. P. Proukakis, A. J. Youd, and D. H. Wacks, "Nonclassical velocity statistics in a turbulent atomic bose-einstein condensate," Phys. Rev. Lett. 104, 075301 (2010).
- [34] H. Adachi and M. Tsubota, "Numerical study of velocity statistics in steady counterflow quantum turbulence," Phys. Rev. B 83, 132503 (2011).
- [35] A. W. Baggaley, "The sensitivity of the vortex filament method to different reconnection models," J. Low Temp. Phys. 168, 18–30 (2012).
- [36] D. Ben-Avraham and S. Havlin, Diffusion and Reactions in Fractals and Disordered Systems (Cambridge University Press, Cambridge, United Kingdom, 2000).
- [37] Y. Sagi, M. Brook, I. Almog, and N. Davidson, "Observation of anomalous diffusion and fractional self-similarity in one dimension," Phys. Rev. Lett. 108, 093002 (2012).
- [38] T. H. Harris, E. J. Banigan, D. A. Christian, C. Konradt, E. D. Tait Wojno, K. Norose, E. H. Wilson, B. John, W. Weninger, A. D. Luster, et al., "Generalized lévy walks and the role of chemokines in migration of effector CD8+ T cells," Nature 486, 545-548 (2012).
- [39] V. Zaburdaev, S. Denisov, and J. Klafter, "Lévy walks," Rev. Mod. Phys. 87, 483–530 (2015).
- [40] J. P. Bouchaud and A. Georges, "Anomalous diffusion in disordered media: Statistical mechanisms, models and physical applications," Phys. Rep. 195, 127–293 (1990).
- [41] M. S. Paoletti, M. E. Fisher, K. R. Sreenivasan, and D. P. Lathrop, "Velocity statistics distinguish quantum turbulence from classical turbulence," Phys. Rev. Lett. 101, 154501 (2008).
- [42] A. C. Davison and D. R. Cox, "Some simple properties of sums of randoms variable having long-range dependence," Proc. R. Soc. Lond. A 424, 255–262 (1989).
- [43] I. M. Mazzitelli and D. Lohse, "Lagrangian statistics for fluid particles and bubbles in turbulence," New J. Phys 6, 203–203 (2004).
- [44] W. F. Vinen, "Mutual friction in a heat current in liquid helium II. III. theory of the mutual friction," Proc. Roy. Soc. A 242, 493–515 (1957).
- [45] R. J. Donnelly, Quantized vortices in helium II, Vol. 2 (Cambridge University Press, 1991).
- [46] R. J. Donnelly and C. F. Barenghi, "The observed properties of liquid helium at the saturated vapor pressure," J. Phys. Chem. Ref. Data 27, 1217–1274 (1998).
- [47] D. Kivotides, J. C. Vassilicos, D. C. Samuels, and C. F. Barenghi, "Kelvin waves cascade in superfluid turbulence," Phys. Rev. Lett. 86, 3080–3083 (2001).
- [48] J. Gao, W. Guo, and W. F. Vinen, "Determination of the effective kinematic viscosity for the decay of quasi-classical turbulence in superfluid $^4{\rm He}$," Phys. Rev. B **94**, 094502 (2016).
- [49] J. Gao, W. Guo, S. Yui, M. Tsubota, and W. F. Vinen, "Dissipation in quantum turbulence in superfluid He above 1 k," Phys. Rev. B 97, 184518 (2018).

Supplemental Materials for: Universal anomalous diffusion of quantized vortices in ultra-quantum turbulence

Satoshi Yui, 1,* Yuan Tang, 2,3,* Wei Guo, 2,3,† Hiromichi Kobayashi, 4,5,‡ and Makoto Tsubota 6,§

1 Department of Physics, Osaka Metropolitan University,
3-3-138 Sugimoto, Sumiyoshi-ku, Osaka 558-8585, Japan

2 National High Magnetic Field Laboratory, 1800 East Paul Dirac Drive, Tallahassee, Florida 32310, USA

3 Mechanical Engineering Department, FAMU-FSU College of Engineering,
Florida State University, Tallahassee, Florida 32310, USA

4 Research and Education Center for Natural Sciences, Keio University,
4-1-1 Hiyoshi, Kohoku-ku, Yokohama 223-8521, Japan

5 Department of Physics, Keio University, 4-1-1 Hiyoshi, Kohoku-ku, Yokohama 223-8521, Japan

6 Department of Physics & Nambu Yoichiro Institute of Theoretical and Experimental Physics
(NITEP) & The OCU Advanced Research Institute for Natural Science and Technology (OCARINA),
Osaka Metropolitan University, 3-3-138 Sugimoto, Sumiyoshi-ku, Osaka 558-8585, Japan

I. VORTEX FILAMENT METHOD

In the framework of the vortex filament model [S1], all the quantized vortex lines are represented by zero-thickness filaments. These filaments are discretized into a series of points with a spatial separation $\Delta \xi$ in the range of $\Delta \xi_{min} = 0.008$ mm to $\Delta \xi_{max} = 0.024$ mm in our simulations. In the absence of the viscous normal fluid, a vortex-filament point at s moves at the local superfluid velocity $\mathbf{v}_s(\mathbf{s})$ as:

$$\frac{d\mathbf{s}}{dt} = \mathbf{v}_s(\mathbf{s}) = \mathbf{v}_0(\mathbf{s}) + \mathbf{v}_{in}(\mathbf{s}), \tag{S1}$$

where $\mathbf{v}_0(\mathbf{s})$ is the applied background superfluid velocity and $\mathbf{v}_{in}(\mathbf{s})$ denotes the velocity induced at \mathbf{s} by all the vortices according to the Boit-Savart law [S1]:

$$\mathbf{v}_{in}(\mathbf{s}) = \frac{\kappa}{4\pi} \int \frac{(\mathbf{s_1} - \mathbf{s}) \times d\mathbf{s_1}}{|\mathbf{s_1} - \mathbf{s}|^3},$$
 (S2)

where the integration is supposed to be performed along all the vortex filaments. However, since the integrant diverges at **s** for an ideal zero-thickness filament, we follow Adachi *et al.* [S2] and calculate the integral as the sum of the local contribution and the non-local contribution:

$$\mathbf{v}_{in}(\mathbf{s}) = \beta_l \mathbf{s}' \times \mathbf{s}'' + \frac{\kappa}{4\pi} \int_{-\infty}^{\infty} \frac{(\mathbf{s_1} - \mathbf{s}) \times d\mathbf{s_1}}{|\mathbf{s_1} - \mathbf{s}|^3}, \quad (S3)$$

where the prime denotes the derivative with respect to the arc length of the vortex filament at \mathbf{s} (i.e., \mathbf{s}' being the unit vector along the filament, and \mathbf{s}'' being the unit vector in the binormal direction divided by the local curvature radius [S1]), and the non-local term represents the integral along the rest of the filament and all other vortices. The coefficient β_l is given by [S1]:

$$\beta_l = \frac{\kappa}{4\pi} \ln \left(\frac{2(l_+ l_-)^{1/2}}{e^{1/4} a_0} \right)$$
 (S4)

where l_+ and l_- are the distances from the point at s to its two nearest neighbour points along the same filament, and the cut-off parameter $a_0 \simeq 1$ Å denotes the vortex core radius in He II. At finite temperatures, the vortices also experience a mutual friction force from the viscous normal fluid. The equation of motion of the vortex-filament points is then given by Eq. (3) in the main paper.

In our ring-injection simulations, the normal-fluid velocity is set to $\mathbf{v}_n = 0$ and so is the background superfluid velocity $\mathbf{v}_0 = 0$. On the other hand, in the counterflow simulations we set $\mathbf{v}_n = U_n \hat{\mathbf{e}}_z$ and $\mathbf{v}_0 = -U_s \hat{\mathbf{e}}_z$. The time evolution of the vortices can be obtained through a temporal integration of the Eq. (1) or the Eq. (3) in the main paper using the fourth-order Runge-Kutta method [S3] with a time step $\Delta t = 10^{-4}$ s. We have confirmed that our spatial and time resolutions are sufficient such that the simulation results are independent of the resolutions. In the evolution of the vortex tangle, whenever two vortex filaments approach to have a minimum separation less than $\Delta \xi_{min}$, we reconnect the two filaments at the location of the minimum separation following the procedures as detailed in ref. [S4, S5]. Furthermore, to maintain the spatial resolution along the filaments, at each time step we delete (or insert) a vortex-filament point between any two adjacent points that have a separation $\Delta \xi < \Delta \xi_{min}$ (or $\Delta \xi > \Delta \xi_{max}$). In all of our simulations, we also remove small vortex loops with lengths less than $5\Delta \xi_{min}$ to account for the cascade loss of the vortices [S4].

II. RANDOMNESS OF VORTEX TANGLE

As discussed in the main paper, ultra-quantum turbulence can be induced by a random tangle of quantized vortices. To check whether the tangles that we presented

^{*} Equal contributions

[†] Email: wguo@magnet.fsu.edu

[‡] Email: hkobayas@keio.jp

[§] Email: tsubota@osaka-cu.ac.jp

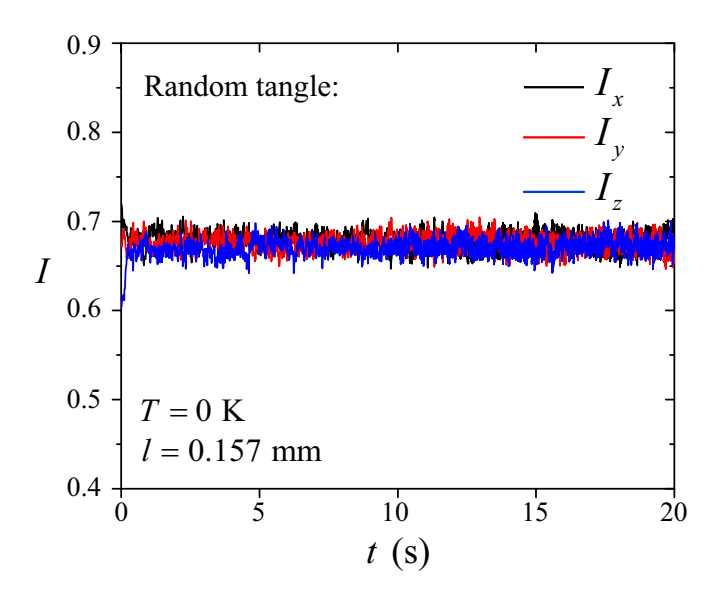


FIG. S1. The vortex-tangle anisotropy parameter I as a function of time t for a representative random vortex tangle produced by injection of vortex rings at T=0 K.

in the paper are indeed random, we may evaluate the dimensionless anisotropy parameter as commonly adopted in the literature [S2]:

$$I_i = \frac{1}{\Omega L} \int_L \left[1 - (\mathbf{s}' \cdot \hat{\mathbf{e}}_i)^2 \right] d\xi, \tag{S5}$$

where L is the vortex-line density (i.e., the total length of the vortices divided by the total volume Ω of the computational box), s' is the unit vector along a vortex segment $d\xi$, $\hat{\mathbf{e}}_i$ is the unit vector in the direction of the axis i (where i = x, y, z), and the integral goes over all the vortex lines in the volume Ω . If the vortex tangle is isotropic, one should expect $I_x = I_y = I_z = 2/3$. On the other hand, in the extreme case that all the vortices are polarized to be perpendicular to the *i*-axis, $I_i = 1$. In Fig. S1, we show the calculated I_x , I_y , and I_z values as functions of the evolution time t for a representative random tangle produced by vortex-ring injection at T = 0 K in our simulation. It is clear that I_x , I_y , and I_z quickly evolve to values close to 2/3, suggesting excellent isotropy of the tangle starting from short evolution times. This result confirms that the method we have adopted for producing the vortex tangle, i.e., by starting with randomly oriented and located vortex rings and by repetitively injecting randomly oriented vortex rings, can efficiently generate and sustain a random vortex tangle.

III. VORTEX-POINT TRACKING

In order to study the apparent diffusion of the vortexfilament points, we give every point a unique index so that it can be identified and tracked during its lifetime. However, tracking a vortex-filament point for long times

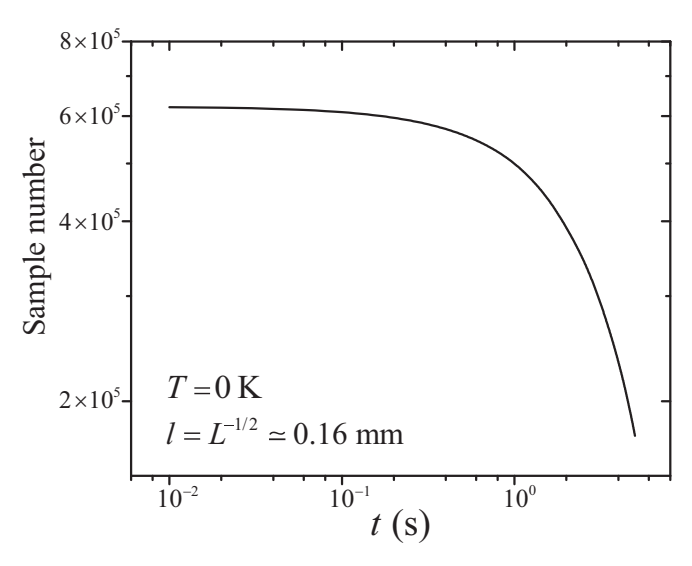


FIG. S2. Sample number versus diffusion time t for a representative case at T=0 K with $\ell=0.16$ mm.

(i.e., over a second) is very challenging. This is because as we adjust the spatial resolution along the vortex filaments at each time step, some vortex-filament points are removed and new points are added. A given vortexfilament point can hardly survive many time steps, which limits the number of samples at large diffusion times. To mitigate this issue, in our typical simulation we randomly tag 200 vortex-filament points in the tangle. When a tagged point and its nearest neighbour point have a separation less than $\Delta \xi_{min}$, we always retain the tagged point and remove its nearest neighbour. This procedure can significantly increase the lifetime of the tagged vortexfilament points. Nevertheless, these tagged points may still get removed in some situations. For instance, when two adjacent points are both tagged points with a separation less than $\Delta \xi_{min}$, one of them will be removed. Furthermore, if a tagged point exists in a vortex loop with a length less than $5\Delta \xi_{min}$, it will be removed together with the loop. Finally, due to the vortex reconnection procedures [S4, S5], there is a certain chance that a tagged point may get removed when it is involved in a reconnection event. Whenever a tagged point is removed, we randomly choose a new point to tag so that there are always 200 tagged points at every time step. Nonetheless, due to the aforementioned loss mechanisms, the averaged lifetime of the tagged points is still limited to few seconds.

When we calculate the mean square displacement (MSD) $\langle \Delta x^2(t) \rangle = \langle [x(t_0+t)-x(t_0)]^2 \rangle$, the number of vortex trajectories for ensemble averaging drops with increasing the diffusion time t. Fig. S2 shows a representative curve of the sample number versus t. Clearly, the sample number drops drastically as t becomes greater than 1 s, which limits the range of the normal diffusion regime and increases the uncertainty of the fitted exponent γ_2 . Another factor that also limits the accuracy of γ_2 is our computational box size. Note that our box size

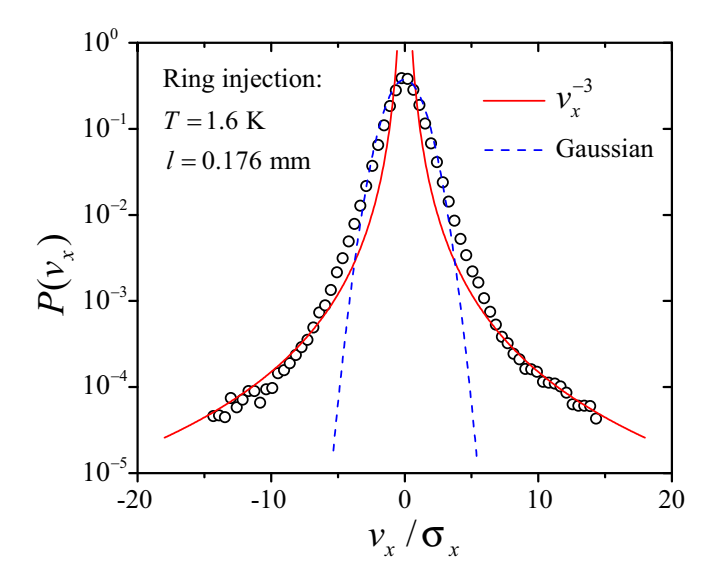


FIG. S3. A representative calculated probability density function $P(v_x)$ of the vortex velocity v_x in the x-direction. The analysis was performed for the random vortex tangle produced by ring injections at 1.6 K with $\ell=0.176$ mm.

(i.e., 1 mm) is not too much larger than the typical line spacing ℓ . Therefore, the vortex tangle is non-uniform at large scales even for tangles produced by random ring injections. Some large-scale variations of the vortex tangle can be clearly seen in Fig. 1 (a) in the main paper. This non-uniformity can lead to sizeable variations of γ_2 in the three axial directions.

IV. VORTEX RECONNECTION AND DISPLACEMENT DISTRIBUTION

For systems involving random walkers, it has been known that the superdiffusion can emerge as a consequence of the so-called Lévy flights, i.e., long-distance hops of the walkers [S6]. In a short time interval Δt , if one measures the displacement $\Delta x = x(t_0 + \Delta t) - x(t_0)$ of the random walkers and calculates the displacement distribution $P(\Delta x, \Delta t)$, this distribution usually exhibits power-law tails $P(\Delta x, \Delta t) \propto |\Delta x|^{-\alpha}$ with $\alpha < 3$ as caused by the Lévy events [S6]. After many steps, the resulted displacement distribution $P(\Delta x, t)$ can converge to a standard Lévy distribution with the same power-law tails [S7]. Mathematically, these flat tails would cause the MSD $\langle \Delta x^2 \rangle$ of the walkers to diverge. However, one may introduce a pseudo MSD through a scaling argument and derive that $\langle \Delta x^2(t) \rangle \propto t^{\gamma}$ with $\gamma = \frac{2}{\alpha - 1}$ [S7]. Therefore, an apparent superdiffusion of the walkers (i.e., $\gamma > 1$) can emerge when $\alpha < 3$. On the other hand, if the tails of $P(\Delta x, \Delta t)$ is not sufficiently flat (i.e., if $\alpha \geq 3$), the central limit theorem then warrants a Gaussian distribution of $P(\Delta x, t)$, which would then lead to a normal diffusion of the walkers [S7].

For quantized vortices in a random vortex tangle in He

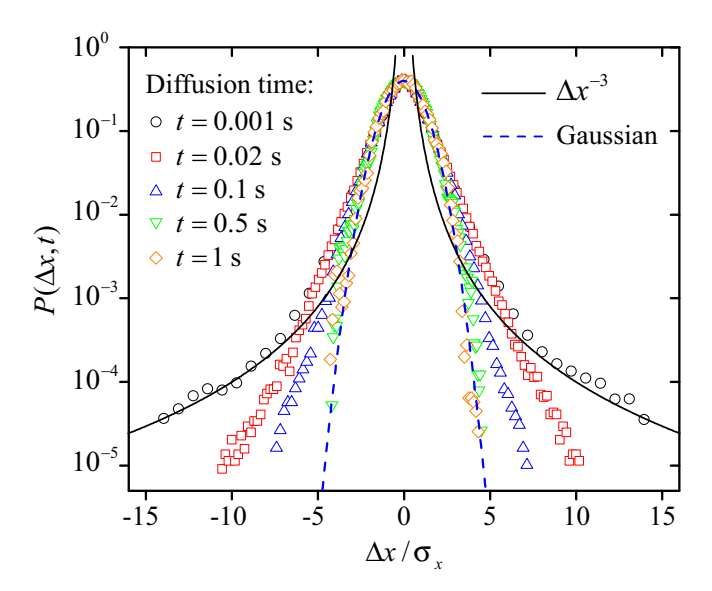


FIG. S4. Vortex-point displacement distribution $P(\Delta x, t)$ at various diffusion time t. The analysis was performed for the same vortex-tangle case as in Fig. S3.

II, the vortex-filament points move chaotically as controlled by both the local superfluid velocity induced by all the vortices and the mutual friction force from the normal-fluid component [S8]. Interestingly, the vortexfilament points do exhibit occasional long-distance hops over short time intervals when they are sufficiently close to other vortex filaments or are involved in vortex reconnections [S9]. This is because when the vortex-filament points are close to the cores of other vortices, the induced velocity according to the Biot-Savart law can become exceptionally large [S8]. These high vortex-velocity occurrences are known to lead to non-Gaussian $|v|^{-3}$ tails of the vortex-velocity distribution [S9, S10]. In Fig. S3, we show the calculated probability density function (PDF) $P(v_x)$ of the vortex velocity v_x in the x-direction for a representative tangle produced by ring injections at 1.6 K with $\ell=0.176$ mm. This PDF is generated by analyzing the velocities of all the tracked vortex-filament points in the steady-state time window. The $|v_x|^{-3}$ tails are clearly visible. Similar results were reported for vortices in a drop of Bose-Einstein Condensate [S11] and in He II counterflow turbulence [S12]. Since the displacement of a vortex-filament point over a short time interval Δt is $\Delta x = v_x \cdot \Delta t$, the displacement distribution of the vortex-filament points should acquire similar power-law tails $P(\Delta x, \Delta t) \propto |\Delta x|^{-3}$.

However, these flat tails of $P(\Delta x, \Delta t)$ do not lead to the superdiffusion of the vortices. This is because the velocities of the vortex-filament points drop rapidly as they move away from nearby vortex cores or the reconnection sites. Therefore, over longer time t the total displacement of a vortex-filament point $\Delta x = \int_0^t v_x(t')dt'$ would rarely exhibit exceptionally large values. As a consequence, the tails of $P(\Delta x, t)$ are gradually suppressed as t increases.

To see this effect, we show in Fig. S4 the calculated displacement distribution $P(\Delta x,t)$ at various diffusion time t for the same vortex-tangle case as presented in Fig. S3. At the smallest diffusion time $t=10^{-3}$ s, $P(\Delta x,t)$ exhibits clear $|\Delta x|^{-3}$ power-law tails, which reflects the $|v_x|^{-3}$ tails of the vortex velocity distribution. But as t increases to over 0.5 s, these power-law tails are suppressed to nearly a Gaussian form. This $P(\Delta x,t)$ behavior was also observed experimentally [S13]. Therefore, despite the existence of some long-distance hops of the vortex-filament points at small time steps, their statistical weight is not sufficient to render the observed vortex superdiffusion. The true mechanism is the vortex veloc-

ity temporal correlation as discussed in the main text.

V. SUPPLEMENTAL MOVIES

Movie S1: Evolution of the vortex filaments in a random tangle produced by vortex-ring injections at 0 K with a steady-state mean vortex-line spacing $\ell = 0.188$ mm. The red dots represent the tracked vortex-filament points for diffusion analysis.

Movie S2: Evolution of the vortex filaments in a tangle produced by counterflow at 1.6 K with a steady-state mean vortex-line spacing $\ell=0.205$ mm. The red dots represent the tracked vortex-filament points for diffusion analysis.

- [S1] K. W. Schwarz, Three-dimensional vortex dynamics in superfluid ⁴He: Homogeneous superfluid turbulence, Phys. Rev. B 38, 2398 (1988).
- [S2] H. Adachi, S. Fujiyama, and M. Tsubota, Steady-state counterflow quantum turbulence: Simulation of vortex filaments using the full biot-savart law, Phys. Rev. B 81, 104511 (2010).
- [S3] W. H. Press, B. P. Flannery, S. A. Teukolsky, and W. T. Vetterling, *Numerical Recipes in C. The Art of Scientific Computing* (Cambridge University Press, Cambridge, 1992).
- [S4] M. Tsubota, T. Araki, and S. K. Nemirovskii, Dynamics of vortex tangle without mutual friction in superfluid ⁴He, Phys. Rev. B 62, 11751 (2000).
- [S5] A. W. Baggaley, The sensitivity of the vortex filament method to different reconnection models, J. Low Temp. Phys. 168, 18 (2012).
- [S6] V. Zaburdaev, S. Denisov, and J. Klafter, Lévy walks, Rev. Mod. Phys. 87, 483 (2015).
- [S7] J.-P. Bouchaud and A. Georges, Anomalous diffusion in disordered media: Statistical mechanisms, models and physical applications, Phys. Rep. 195, 127 (1990).

- [S8] R. J. Donnelly, Quantized vortices in helium II, Vol. 2 (Cambridge University Press, 1991).
- [S9] M. S. Paoletti, M. E. Fisher, K. R. Sreenivasan, and D. P. Lathrop, Velocity statistics distinguish quantum turbulence from classical turbulence, Phys. Rev. Lett. 101, 154501 (2008).
- [S10] B. Mastracci and W. Guo, Characterizing vortex tangle properties in steady-state He II counterflow using particle tracking velocimetry, Phys. Rev. Fluids 4, 023301 (2019).
- [S11] A. C. White, C. F. Barenghi, N. P. Proukakis, A. J. Youd, and D. H. Wacks, Nonclassical velocity statistics in a turbulent atomic bose-einstein condensate, Phys. Rev. Lett. 104, 075301 (2010).
- [S12] H. Adachi and M. Tsubota, Numerical study of velocity statistics in steady counterflow quantum turbulence, Phys. Rev. B 83, 132503 (2011).
- [S13] Y. Tang, S. Bao, and W. Guo, Superdiffusion of quantized vortices uncovering scaling laws in quantum turbulence, Proc. Natl. Acad. Sci. U.S.A 118, e2021957118 (2021).